Journal of Rare Earths xxx (xxxx) xxx

Contents lists available at ScienceDirect

Journal of Rare Earths

journal homepage: http://www.journals.elsevier.com/journal-of-rare-earths

A mechanic insight into low-temperature catalytic combustion toward ethylene oxide over Pt-Ru/$CuCeO_x$ bimetallic catalyst☆

Wenxi Zhou [a], Kai Chen [a], Quanli Ke [a], Haoru Wang [a], Xiao Chen [b], Yufeng Liu [a], Guokai Cui [a], Xiaole Weng [c], Ying Zhou [a, **], Hanfeng Lu [a, *]

[a] Institute of Catalytic Reaction Engineering, College of Chemical Engineering, Zhejiang University of Technology, Huzhou, 313200, China
[b] Department of Safety and Environmental Protection, Pharmaceutical College, Jinhua Polytechnic, Jinhua, 321017, China
[c] Key Laboratory of Environment Remediation and Ecological Health, Ministry of Education, College of Environmental and Resource Sciences, Zhejiang University, Hangzhou, 310058, China

ARTICLE INFO

Article history:
Received 28 September 2022
Received in revised form
14 March 2023
Accepted 20 March 2023
Available online xxx

Keywords:
Ethylene oxide
Bimetallic catalyst
Catalytic oxidation
Degradation pathway
Mechanism
Rare earths

ABSTRACT

The catalytic oxidation performance toward ethylene oxide (EO) and the consequent mechanism were investigated on the Pt-Ru/$CuCeO_x$ bimetallic catalyst, which was prepared by a distinct method combining stepwise adsorption and subsequent impregnation. The catalytic tests show that the introduction of Ru into the Pt catalyst, so as to form Pt-Ru bimetallic active sites, can greatly increase the oxidation activity of the catalyst, as evidenced by the extremely lower full oxidation temperature (120 °C) when compared with that of the Pt/CeO_2 catalyst (160 °C). The XPS spectra show that the Ru species (mainly RuO_x) have strong interaction with the $CuCeO_x$ support, which can therefore affect the electron transfer between the Pt species and the support. As a result, the oxygen activation on Pt species is obviously facilitated and catalytic activity is enhanced. Finally, *in situ* diffuse reflectance infrared Fourier transform spectroscopy (DRIFTs) was used to track the reaction mechanism. It is found that the catalytic oxidation process follows the MvK catalytic mechanism at low temperature and the L-H catalytic mechanism when the temperature moves to higher range.

1. Introduction

Ethylene oxide (EO) is a new generation of excellent fungicide and disinfectant. Because of its effectiveness and compatibility, it is widely used for sterilization and disinfection in the medical industry.[1] However, the residual EO gas in disinfection devices is a serious threat to both the environment and human health (WHO List of Carcinogens, 2012, category I).[2] Among the treatment technology for EO waste gas, the water absorption technology is usually adopted in the industry, especially with the assistance of acid catalysts. Therein, EO waste gas is first dissolved in water, and then catalytically transformed into ethylene glycol and other polyols under low temperature, so as to eliminate the pollution of EO waste gas.[3–9] Although catalytic absorption technology has some advantages such as low operating expenses, it will also produce a large amount of waste liquid (polyols) and spent catalyst, resulting in secondary pollution. Therefore, a more efficient and environment-friendly abatement way is urgently needed.

Catalytic combustion technology owns the merits of high efficiency and environmental compatibility, which can completely convert EO into harmless CO_2 and H_2O.[10–12] The key to catalytic combustion is the development of catalysts. Meanwhile, the spontaneous combustion point temperature of EO is low (429 °C), which gives rise to safety concerns. In order to address the safety and energy consumption of the catalytic combustion system, it is necessary to develop a low-temperature catalytic combustion catalyst. Previously our group has carried out in-depth research about the EO catalytic oxidation on various oxide catalysts and noble metal catalysts, and observed the superior activity of Pt/CeO_2 catalyst at low temperature (less than 160 °C) to the commercial Pt/Al_2O_3 catalyst (>200 °C).[13] However, the metal-support interaction is still an ambiguous problem, which is worthy of further research to adjust the interface and improve the activity and stability of the

☆ **Foundation item**: Project supported by the National Natural Science Foundation of China (22208300, 22078294, 21922607) and Natural Science Foundation of Zhejiang Province (LZ21E080001, LGF20E080018).
* Corresponding author.
** Corresponding author.
E-mail addresses: wjfx@zjut.edu.cn (Y. Zhou), luhf@zjut.edu.cn (H. Lu).

https://doi.org/10.1016/j.jre.2023.03.016
1002-0721/© 2023 Published by Elsevier B.V. on behalf of Chinese Society of Rare Earths.

catalysts. In order to realize this target, bimetallic catalysts have proven to show excellent catalytic activity due to the synergistic effect between different metals.[14–16] After screening, Ru was found to be a good candidate which could have good cooperation with Pt when coexisting on the support surface. For example, Wang et al. found that $Pt_{0.7}Ru_{0.3}/ZrO_2$ catalyst has a high oxygen adsorption capacity, and the Pt-Ru bimetallic sites jointly promote the activation of oxygen molecules, which can accelerate the catalytic oxidation of toluene.[17] Next to that, Serna-Mata et al. found that Pt-Ru/C demonstrated high activity in ethanol oxidation reaction and enhanced tolerance to CO poisoning, owing to the formation of Pt-Ru alloyed phases.[18] Besides, Mao et al. found that in counterparts with similar structure CeO_2 (an O_x^{n-} generator) and Pr_6O_{11} (a lattice oxygen contributor), it is suggested that the catalytic combustion of propane under lean-burn conditions followed a typical Mars-van Krevelen mechanism, in which catalyst lattice oxygen represented the dominant reactive phases.[19] Cu is a remarkable promoter for many volatile organic compounds (VOCs) degradation reactions, such as oxidation of acetone, toluene and pyrene, when doping into the support.[20–22] Given this, it is strongly anticipated that the introduction of Ru species in the Pt metal phase and Cu into the lattice of CeO_x support could greatly benefit the electron transfer between the metal and support, and thus exhibit even better activity than the reference Pt/CeO_x catalyst.

Herein, a highly efficient Pt-Ru/$CuCeO_x$ catalyst was prepared for the catalytic oxidation of EO. In comparison to the benchmark Pt/CeO_2 catalyst, the introduction of a second active Ru phase to Pt phase, as well as the Cu doping in the CeO_x lattice, could markedly enhance the oxygen activation ability of the catalyst and then achieve low-temperature degradation of the EO molecules. Moreover, the reaction mechanism and EO degradation pathway on Pt-Ru/$CuCeO_x$ catalyst were explored by *in situ* diffuse reflectance infrared Fourier transform spectroscopy (DRIFTs). The results show that EO oxidation process fits well with the MvK mechanism and the L-H mechanism, respectively, at low temperature and high temperature.

2. Experimental

2.1. Chemical agents

Cerium nitrate hexahydrate (Macklin; 99.99%), copper nitrate trihydrate (SCR Co., Ltd.; 99.0%), ruthenium trichloride (SCR Co., Ltd.; 37.0%), chloroplatinic acid hexahydrate (Shanghai Jiuyue Chemical Co., Ltd.; 59.0%), hydrazine hydrate aqueous solution (SCR Co., Ltd.; 85%), sodium hydroxide (Shanghai Lingfeng Chemical Reagent Co., Ltd.; 96.0%). All chemicals of analytical grade were used as received without further purification.

2.2. Catalyst preparation

2.2.1. Preparation of $CuCeO_x$

Mixed metal oxides were prepared by co-precipitation method with NaOH as precipitator. Under vigorous agitation, the NaOH solution was added drop by drop to a mixture of the two nitrates with a molar ratio of Cu:Ce = 1:99 (The reason for choosing this ratio is shown in Fig. S1), and the pH was adjusted to 9–11. The mixture was then stirred for 3 h, left to age overnight, dried at 110 °C for 12 h, and finally calcined at 500 °C for 3 h. The other composite oxides in Fig. S2(b) were prepared using the same ratio and process.

2.2.2. Preparation of Pt/$CuCeO_x$

The required amount of chloroplatinic acid solution (c(Pt) = 0.015 mol/L) was first dissolved in 20 mL of deionized water. Then 1 g $CuCeO_x$ powder was added to the chloroplatinic acid solution and the resulting mixture was stirred in a 75 °C water bath for 1 h. After filtration, the obtained solid was dissolved in another 20 mL of deionized water along with 140 μL of 85% hydrazine hydrate solution. The mixture above was reduced for 1 h and then filtrated, dried at 100 °C for 1 h, and finally calcined at 400 °C for 4 h.

2.2.3. Preparation of Ru/$CuCeO_x$

The desired amount of ruthenium chloride solution (c = 0.025 mol/L) was first dissolved in 20 mL of deionized water. Then 1g $CuCeO_x$ powder was added to the ruthenium chloride solution and the resulting mixture was stirred in a 75 °C water bath for 1 h. Filtered, dried at 100 °C for 1 h, and finally calcined at 400 °C for 4 h. 0.1 wt% Ru/$CuCeO_x$ is denoted as 0.1Ru/$CuCeO_x$. Reduced production for 0.2Ru/$CuCeO_x$, 0.5Ru/$CuCeO_x$ and 1.0Ru/$CuCeO_x$, 1.0Ru/$CuCeO_x$ unreduced production is the same as above.

2.2.4. Preparation of bimetallic Pt-Ru/$CuCeO_x$

The desired amount of chloroplatinic acid solution (c(Pt) = 0.015 mol/L) was first dissolved in 20 mL of deionized water. Then 1g Ru/$CuCeO_x$ powder was added to the chloroplatinate solution, and the resulting mixture was stirred in a 75 °C water bath for 1 h. The resulting solids were filtered and dissolved in an additional 20 mL of deionized water together with 140 μL of 85% hydrazine hydrate solution. The mixture was filtered after reaction for 1 h, dried at 100 °C for 1 h, and finally calcined at 400 °C for 4 h. Preparation of 1.0Ru/$CuCeO_x$-reduced catalyst is the same as above. 0.1Pt/0.1Ru denotes 0.1 wt%Pt/0.1 wt%Ru/$CuCeO_x$. The preparation of 0.1 wt%Pt/0.2 wt%Ru/$CuCeO_x$, 0.1 wt%Pt/0.5 wt%Ru/$CuCeO_x$ and 0.1 wt%Pt/1.0 wt%Ru/$CuCeO_x$ is the same as above. Notably, although the catalysts herein were denoted as bimetallic catalysts, some RuO_x species may also be generated during the final calcination.

2.3. Catalyst characterization

High resolution transmission electron microscopy (HRTEM) and energy dispersive spectroscopy (EDS) were operated on a Tecnai G2 F30 S-Twin electron microscope at 300 kV.

The specific surface area of the catalysts was measured by the Brunauer–Emmett–Teller (BET) method from nitrogen adsorption isotherms. Experiments were carried out on a Micromeritics ASAP 2020 instrument at 77 K. Before experiments, samples were degassed at 423 K for 3 h.

Outlet gases were identified using an Agilent GC 7890B and an Agilent 5977A MS detector (Agilent, Santa Clara, CA, USA). The outlet gas was first collected by the gas sampling bag, and then the gas was released to the GC-MS analyzer.

X-ray photoelectron spectroscopy (XPS) measurements were made on an ESCALAB 250 (Thermo Scientific K-Alpha, USA) high-performance electron spectrometer using Al Kα as the excitation source. The likely charging of samples was corrected by setting the binding energy of the adventitious carbon (C 1s) to 279.18 eV.

In situ DRIFTs of EO oxidation was performed using a Bruker Vertex 70 infrared spectrometer, equipped with a mercury cadmium telluride (MCT) detector cooled by liquid nitrogen. A Harrick reaction cell was fitted with KBr windows and connected to a purging and adsorption gas control system. The total flow rate was controlled by a mass flow meter. Before the catalytic oxidation of EO, the catalyst samples were pretreated under N_2 at 200 °C for 1 h to remove the surface impurities. This spectrum was then subtracted from the corresponding spectrum of the catalyst and reaction mixture in the cell. For the EO oxidation experiment, the catalysts were exposed to a gas mixture consisting of 10000 ppm

EO and air at the temperature range of 80–260 °C. The system reached a steady-state in about 45 min. All spectra were collected at a resolution of 4 cm^{-1} each with 100 scans.

2.4. Catalytic activity test

The performance of prepared materials in the oxidation of EO was investigated in a continuous-flow fixed-bed reactor at atmospheric pressure. In each test, 0.1 g of catalyst was placed into the tube reactor. The EO feed gas was generated by bubbling the EO liquid with air in an ice-water bath. The EO gas was then mixed with certain airflow (79% N_2 + 21% O_2) so that the total flow rate was maintained at 66.67 mL/min (10000 ppm EO and weight hourly space velocity = 40000 mL/(g·h)). The catalyst bed was subsequently set to the desired temperature and left to equilibrium for 20 min before automatic sampling was initiated, as shown in Fig. S3.

The concentrations of EO were measured by gas chromatography (GC-1620; Jiedao, China) equipped with a flame ionization detector (FID) and an RTX-1 column (30 m × 0.25 mm (ID) × 0.25 μm). The conversion of EO (X_{EO}) was calculated as follows:

$$X_{EO} = ([EO]_{in} - [EO]_{out}) / [EO]_{in} \times 100\% \quad (1)$$

where $[EO]_{in}$ and $[EO]_{out}$ represent the EO concentrations in the inlet and outlet gas flows, respectively.

3. Results and discussion

3.1. Catalytic performance evaluation

3.1.1. Catalytic activity of fresh catalysts

As mentioned above, the Ru metal phase and oxide support composition may both affect the catalytic performances. Therefore, an optimization for the Ru valence and support composition was first performed to select the optimal preparation way of the catalysts. As shown, RuO_x species were found more active than its reduced form during the EO oxidation process (Fig. S2(a)), while $CuCeO_x$ was proven a better support than other composite oxides and the sole CeO_2 (Fig. S2(b)). In this consideration, a series of non-reduced Ru/$CuCeO_x$ catalysts with different Ru loading amounts was prepared, wherein those Ru/$CuCeO_x$ samples possessing Ru loading amount higher than 0.5 wt% exhibited superior catalytic activity (T_{90} = 158 °C, Fig. 1(a)). Notably, the catalytic activity of 0.1Ru/$CuCeO_x$ catalyst (T_{90} = 198 °C) is even worse than that of the sole support (T_{90} = 177 °C, Fig. 1(b)), which may be attributed to the reduction of RuO_x species by the Cu^+ within the $CuCeO_x$ support.[23,24] As for the Pt-based catalysts, the light–off curves of Pt/$CuCeO_x$ catalysts with varied Pt loading amounts were also obtained. Similarly, the T_{90} values for EO oxidation were found much lower than those after Pt loading, and the optimum Pt loading amount was 0.1 wt%, as seen in Fig. 1(c and d). Based upon these results, different amounts of Ru were added to Pt/$CuCeO_x$ catalyst with constant Pt amount (0.1 wt%) in order to investigate the impacts of the synergy between the Pt-Ru bimetallic phases on the EO oxidation activity (Fig. 1(e)). As is shown, when Pt and Ru were concurrently present on the $CuCeO_x$ support, the activity of the bimetallic catalysts for EO oxidation was significantly enhanced (Fig. 1(f)). When the Ru loading amount in the bimetallic catalysts was higher than 0.5 wt%, the T_{90} could reach as low as 118 °C, which is 40 °C lower than that of the Pt/CeO_2 catalyst under the same test conditions.[13] Given this, the Pt-Ru bimetallic catalyst was evidenced to have excellent catalytic activity for EO oxidation under low temperature, when loaded on the $CuCeO_x$ support.

3.1.2. Stability of catalyst

In order to study the stability of the 0.1Pt-0.5Ru/$CuCeO_x$ catalyst, the thermal stability and water resistance were first examined by changing the temperature and water vapor concentration during the reaction. As shown in Fig. 2(a), the initial EO conversion rate was *ca.* 60% at reaction temperature of 110 °C. When the reaction temperature increased to 400 °C, the EO conversion rate was stabilized at 100%, and no obvious decrease of activity was detected even after two ramping–cooling cycles, which certifies the superb thermal stability of the catalyst. In a similar way, the water resistance of the catalyst was periodic injection of water vapor at relative humidity (RH) value of 30% (Fig. 2(b)). The 0.1Pt-0.5Ru/$CuCeO_x$ catalyst maintained good catalytic performance (EO conversion rate at *ca.* 100%), either the water vapor is present or absent. Additionally, even with the injection of water vapor, and the activity of the catalyst remains unchanged in the long-term evaluation for about 25 h, which clearly reflects the good water resistance and long lifetime of the catalyst.

Next to the temperature and water vapor concentration, the reaction stability was also tested in terms of different space velocity and substrate concentrations. As shown in Fig. 2(c), the catalytic activity for EO oxidation over 0.1Pt-0.5Ru/$CuCeO_x$ catalyst was investigated at different space velocity (20000–60000 mL/(g·h)). Noticeably, even with a three-fold increase in the space velocity (60000 mL/(g·h)), the 0.1Pt-0.5Ru/$CuCeO_x$ catalyst can still achieve 97% EO conversion at 120 °C, and the T_{90} and T_{100} for EO oxidation at different space velocity are almost unchanged. Likewise, the EO oxidation activity over 0.1Pt-0.5Ru/$CuCeO_x$ catalyst was also evaluated using varied initial EO concentrations (3000–10000 ppm) (Fig. 2(d)). Even when the EO concentration was reduced to 3000 ppm, the catalytic activity was still well remained. All these results indicate that the 0.1Pt-0.5Ru/$CuCeO_x$ catalyst has good (hydro)thermal and structural stability, which makes it promising for future applications.

3.2. Catalysts characterization

The HRTEM and EDS images of fresh 0.1Pt/$CuCeO_x$ and 0.1Pt-0.5Ru/$CuCeO_x$ catalysts are depicted in Fig. 3 (here denoted as Pt/$CuCeO_x$ and Pt-Ru/$CuCeO_x$, and the same after). According to Fig. 3(a), although the amount of Pt (0.1 wt%) is very low, small Pt particles can still be witnessed on the surface of $CuCeO_x$, with little agglomeration. In contrast, when five-fold Ru was added simultaneously with Pt, both Ru and Pt are found more evenly distributed on the surface of $CuCeO_x$ support, which set a good foundation stone for its excellent catalytic activity.

XPS spectra were collected to study the chemical states of $CuCeO_x$, Ru/$CuCeO_x$ and Pt-Ru/$CuCeO_x$ catalysts. When Ru was introduced into the $CuCeO_x$ support, the ratio of Ce^{3+} in the catalyst was found to reduce, quite possibly due to the formation of metal-support interaction by electron transfer from Ce^{3+} to $Ru^{\delta+}$ (Fig. 4(a), Table 1). Besides, the surface areas were also found to decrease, which could be explained by the adsorption and coverage of $Ru^{\delta+}$ cations on the support surface (Table 1). The Ru 3d XPS spectra of the Ru/$CuCeO_x$ and Pt-Ru/$CuCeO_x$ catalysts were further collected to verify the states of Ru on the catalysts. The signals attributed to Ru^0 and $Ru^{\delta+}$ ($0 < \delta \leq 4$) could be well resolved at 285.0 and 281.6 eV, correspondingly, as reported previously.[17] According to the deconvolution results, the main state on the Ru/$CuCeO_x$ catalyst was RuO_x species, which accounts for 36.5% of the total Ru amount (Fig. 4(b), Table 1). This indicates that the presence of RuO_x species is beneficial to the deep oxidation of EO molecules. When the Pt and Ru bimetallic phases were present together, the $Ru^{\delta+}$ content was further increased to 54.1%, which means that more electrons were transferred from Ru to Pt phase, and an enhanced number of

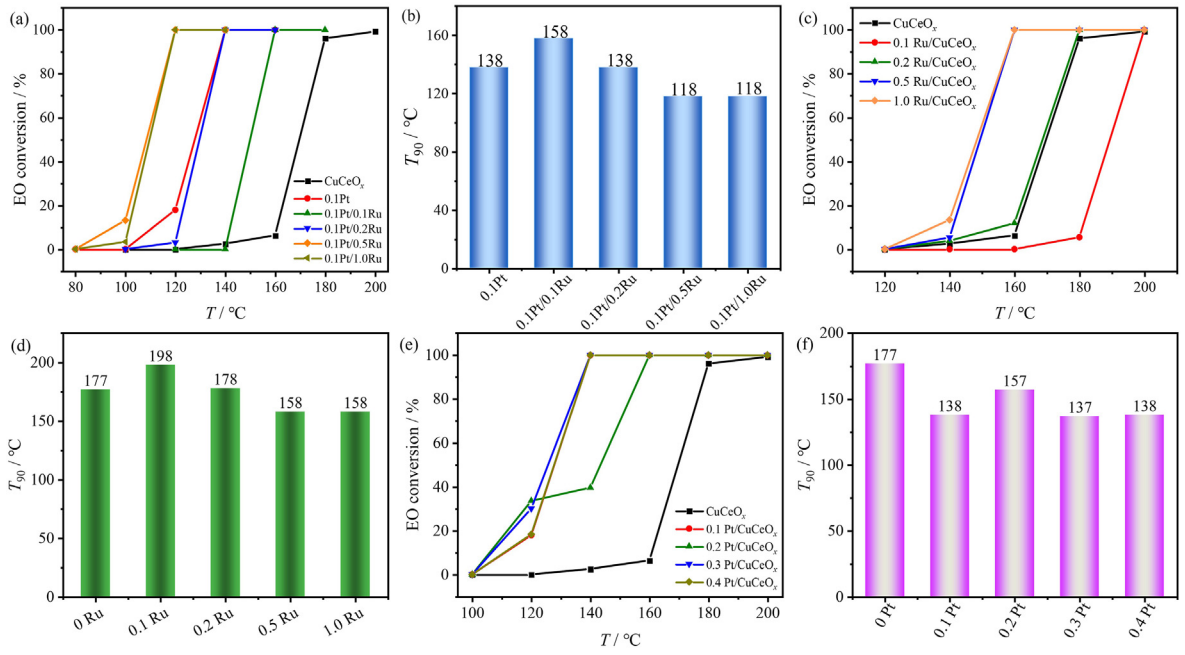

Fig. 1. (a) The influence of Pt-Ru ratios on the EO catalytic activity; (b) The T_{90} values for EO oxidation over catalysts with different Pt-Ru ratios; (c) The EO conversion over Ru-based catalysts with varied Ru loading amounts; (d) The T_{90} values for EO oxidation over Ru-based catalysts with varied Ru loading; (e) The EO conversion over Pt-based catalysts with varied Pt loading; (f) The T_{90} values for EO oxidation over Pt-based catalysts with varied Pt loading amounts.

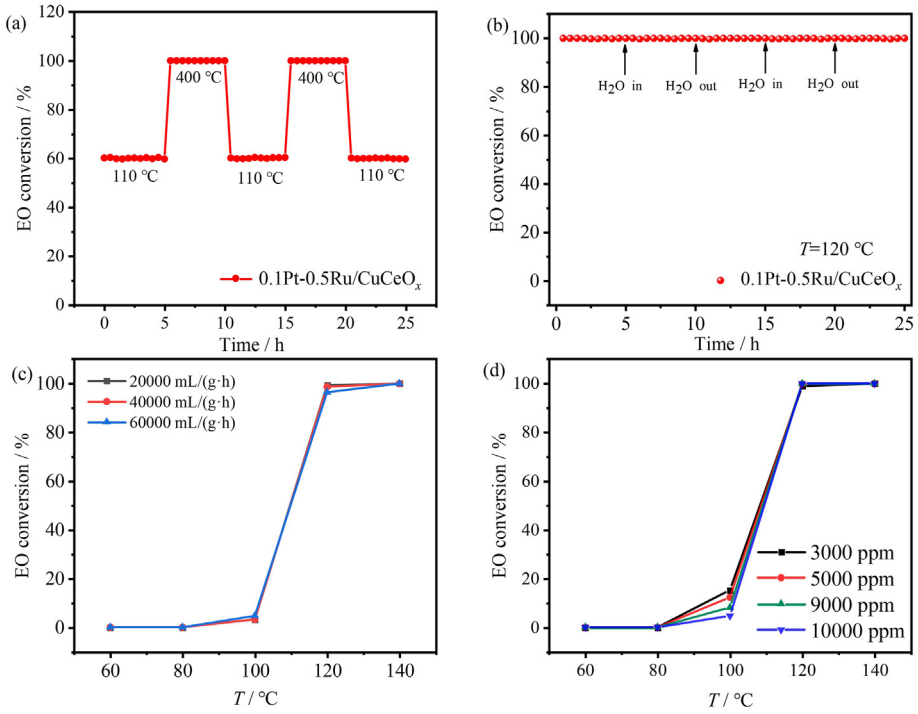

Fig. 2. (a) The thermal stability tests for EO oxidation over 0.1Pt-0.5Ru/$CuCeO_x$ catalyst by consecutive ramping to 400 °C and cooling to 110 °C; (b) The water resistance tests for EO oxidation over 0.1Pt-0.5Ru/$CuCeO_x$ catalyst by consecutive injection of water vapor. Both the temperature ramping and water vapor injection were initiated after reaction for 5 h, and the relative humidity for the water resistance tests was kept at 30%; The EO conversion on 0.1Pt-0.5Ru/$CuCeO_x$ catalyst at different mass space velocities (c) and different initial EO concentrations (d).

RuO_x species could participate in the reaction, accelerate the transformation of intermediate products and improve the catalytic activity. Meanwhile, since more electrons were enriched on the Pt nanoparticles, the adsorption and activation of oxygen molecules were also facilitated, which benefits the catalytic oxidation of EO.

3.3. Mechanism analysis

To explore the degradation pathway of the EO oxidation reaction on the Pt-Ru/$CuCeO_x$ catalyst, the products were analyzed by GC-MS at T_{50} and T_{90} (Fig. S4 and Table 1). At T_{50}, the tail gas

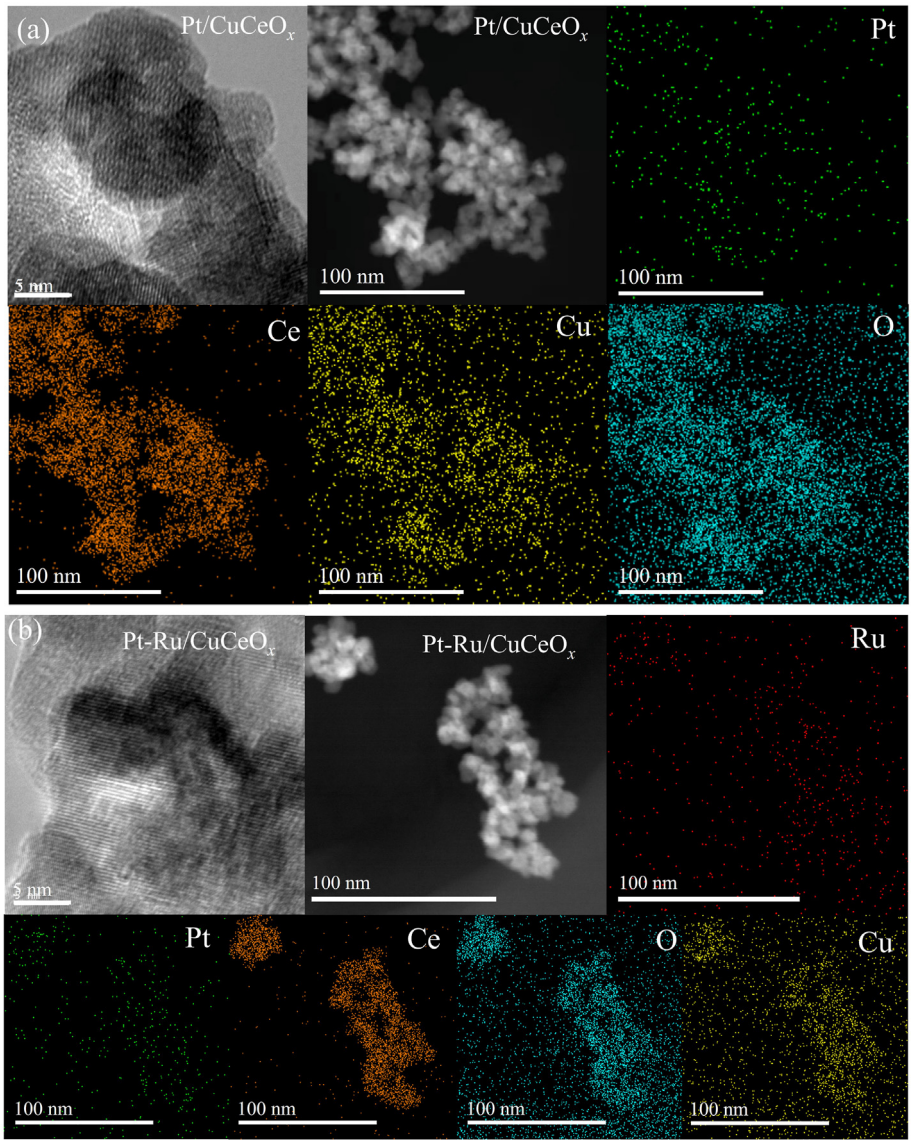

Fig. 3. HRTEM and EDS elemental mapping images of 0.1Pt/CuCeO$_x$ (a) and 0.1Pt-0.5Ru/CuCeO$_x$ (b) catalysts.

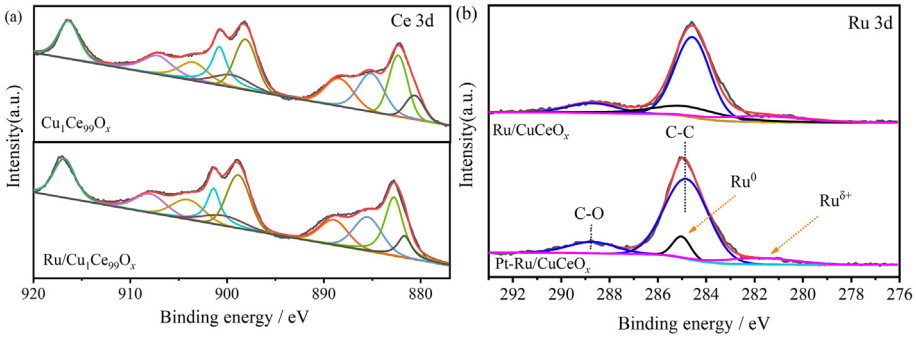

Fig. 4. XPS spectra of Ce 3d of CuCeO$_x$ and Ru/CuCeO$_x$ catalyst (a) and Ru 3d of Ru/CuCeO$_x$ and Pt-Ru/CuCeO$_x$ catalysts (b).

contained acetic acid, acetaldehyde and carbon dioxide. At T_{90}, only acetic acid is a kind of organic matter in tail gas. Ethylene oxide is completely transformed at 120 °C, and there is no organic matter in the tail gas, indicating that the catalyst Pt-Ru/CuCeO$_x$ can completely oxidize ethylene oxide without secondary pollution. Our previous researches have shown different EO adsorption characteristic bands on Pt/Al$_2$O$_3$ catalyst and Pt/CeO$_2$ catalyst surface, so the specific adsorption bands were first examined on the

Table 1
Ce^{3+} and $Ru^{\delta+}$ ratios and product analysis of catalysts.

Samples	S_{BET} (m^2/g)	$Ce^{3+}/(Ce^{3+}+Ce^{4+})$ (%)	$Ru^{\delta+}/Ru^0$ (%)	GC-MS		
				T_{50}	T_{90}	T_{100}
$CuCeO_x$	64.4	31.9	–	–	–	–
$Ru/CuCeO_x$	60.4	30.1	36.5	–	–	–
$Pt\text{-}Ru/CuCeO_x$	90.0	–	54.1	CO_2, CH_3CHO, CH_3COOH	CO_2, CH_3COOH	CO_2

$Pt\text{-}Ru/CuCeO_x$ catalyst at room temperature.[16] As demonstrated in Fig. S5, the peaks at *ca.* 2770–3128 and 1267 cm^{-1} belong to the ν_{as}(C–H) stretching vibration and δ(C–H) bending vibration of methyl (–CH_3) and methylene (–CH_2) groups, while the infrared peaks of *ca.* 1083 and 870 cm^{-1} correspond to the asymmetric ν_{as}(C–O–C) stretching vibration and symmetric ν_s(C–O–C) stretching vibration of EO molecule.[25] The characteristic absorption peak intensity of EO increases with extended feeding of reaction gas, which indicates that EO has good adsorption properties on the surface of $Pt\text{-}Ru/CuCeO_x$ catalyst. Meanwhile, the signals at *ca.* 1558 and 1658 cm^{-1} are ascribed to the carboxylic acid carbonyl species and aldehyde carbonyl species, respectively, which indicates that EO has already been converted into acetaldehyde and then acetic acid on the catalyst surface at room temperature.[26] In addition, the absorption peak at 1809 cm^{-1} corresponds to carbon-based species and originates from the intermediates of the above chemical reactions.[27] Subsequently, the band changes on the catalyst surface were tracked to speculate the degradation process of EO on the surface of $Pt\text{-}Ru/CuCeO_x$ catalyst during the heating process. As the reaction temperature increased to 100 °C, four new absorption peaks were observed, namely 3225, 2715, 1369 and 940 cm^{-1}, which are respectively attributed to surface hydroxyl species, ν_s(C–H) stretching vibration of acetaldehyde, symmetric ν_s(–COOH) stretching vibration of carboxylic acid and δ(C–OH) bending vibration of hydroxyl group, as shown in Fig. 5.[25,28,29] The existence of carboxylic acid vibration peaks at 1558 cm^{-1} (ν_{as}(–COOH)) and 1369 cm^{-1} (ν_s(–COOH)) under 100 °C indicates

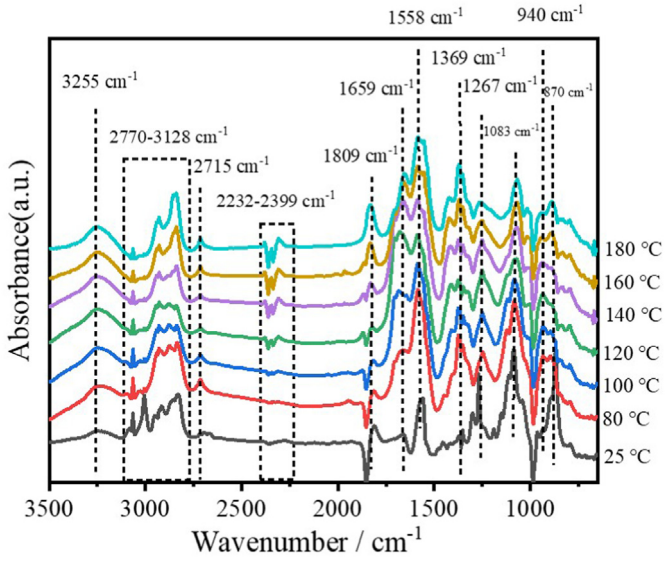

Fig. 5. *In situ* DRIFTs spectra of EO catalytic oxidation on $Pt\text{-}Ru/CuCeO_x$ catalyst surface. The EO was injected with air at different temperatures. The inlet EO concentration was maintained at 10000 ppm and the weight hourly space velocity at 40000 mL/(g·h). The signals related to carbonyl (C=O) vibration (*ca.* 1585 cm^{-1}), aldehyde carbonyl group (*ca.* 1658 cm^{-1}), carboxylic acid carbonyl (*ca.* 1558 cm^{-1}) carboxyl group (*ca.* 1369 cm^{-1}) and CO_2 vibration (2232–2399 cm^{-1}) are the most important ones.

that acetic acid may exist in the form of acetate on the surface of $Pt\text{-}Ru/CuCeO_x$ catalyst. The presence of the stable carboxylate could hinder the deep catalytic oxidation of acetic acid during the heating process.[30] Therefore, the degradation of acetic acid may be the controlling step of EO catalytic oxidation on $Pt\text{-}Ru/CuCeO_x$ catalyst surface. When the temperature increased to above 120 °C, the enhancement of the characteristic absorption peaks at 2232–2399 cm^{-1} is attributed to the CO_2 species, which refers to the conversion of acetic acid to CO_2 and H_2O. Therefore, EO adsorbed on the surface of $Pt\text{-}Ru/CuCeO_x$ catalyst can be partially oxidized at low temperature, and converted to intermediate products (acetic acid) even at room temperature. When the temperature rises to 100 °C, EO starts to be transformed into CO_2 and H_2O, showing excellent catalytic activity at low temperature.

In order to further understand the catalytic mechanism of EO on the surface of $Pt\text{-}Ru/CuCeO_x$ catalyst, the reaction atmosphere was switched at T_{10} (95 °C) and T_{100} (120 °C) respectively, and the changes of the bands on the surface of the catalyst were tested. Under the condition of nitrogen only, stretching vibration attributed to carboxyhydroxyl group of acetate (3064 cm^{-1}) and C–H bond in acetaldehyde (2715 cm^{-1}) were detected, indicating that EO was converted to acetaldehyde and then acetic acid on the surface of the catalyst.[25] When the reaction gas is switched to air during the reaction, the absorption peaks of acetic acid and acetaldehyde are basically unchanged (Fig. 6(a)). After 40 min, the reaction gas was recovered to nitrogen, and the absorption peak attributed to acetic acid was enhanced, while that of acetaldehyde was hardly observed. This is possibly because the previous air intake triggered the acetaldehyde conversion to acetic acid, which obviously follows the catalytic mechanism of MvK (Mars-van Krevelen).[31] Interestingly, the same experimental procedure at T_{100} showed completely different phenomena, as shown in Fig. 6(b). The characteristic peak of acetaldehyde could be hardly observed either with nitrogen or air as the reaction gas. In the presence of nitrogen only, the characteristic peaks of acetic acid can be obviously observed (till 40 min). When the air was injected instead, the absorption peak assigned to acetic acid immediately disappeared, which implies that acetic acid was converted to CO_2 and H_2O on the surface of the catalyst. When the reaction gas switches back to nitrogen again, the absorption peak assigned to acetic acid appears again, which fits well with the Langmuir–Hinshelwood (L-H) catalytic mechanism.[32] In conclusion, both MvK and L-H catalytic mechanisms exist on the surface of $Pt\text{-}Ru/CuCeO_x$ catalysts, depending on the varied atmosphere and temperature, which jointly promote the deep catalytic oxidation of EO.

In summary, the possible degradation mechanism of EO on the surface of $Pt\text{-}Ru/CuCeO_x$ catalyst was proposed, as shown in Fig. 7. EO is firstly adsorbed on the surface of the catalyst, where β-H transfer occurs when EO molecules bond with the surface of the support, and then EO is converted into acetaldehyde. Thereafter, acetaldehyde is quickly oxidized into acetic acid by the lattice oxygen of $CuCeO_x$, and this process follows the MvK catalytic mechanism. In the meantime, molecular oxygen is adsorbed and dissociated (or activated) at the active sites of noble metal Pt-Ru nanoparticles, and the obtained oxygen anion migrates to the

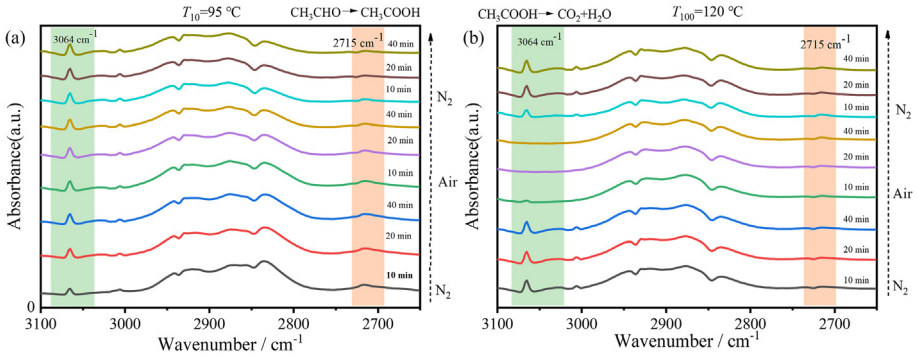

Fig. 6. *In situ* DRIFTs spectra of EO catalytic oxidation on the surface of Pt-Ru/$CuCeO_x$ catalysts at constant temperature of T_{10} = 95 °C (a) and T_{100} = 120 °C (b). The spectra in both tests were collected with extended time and switch of atmospheric conditions.

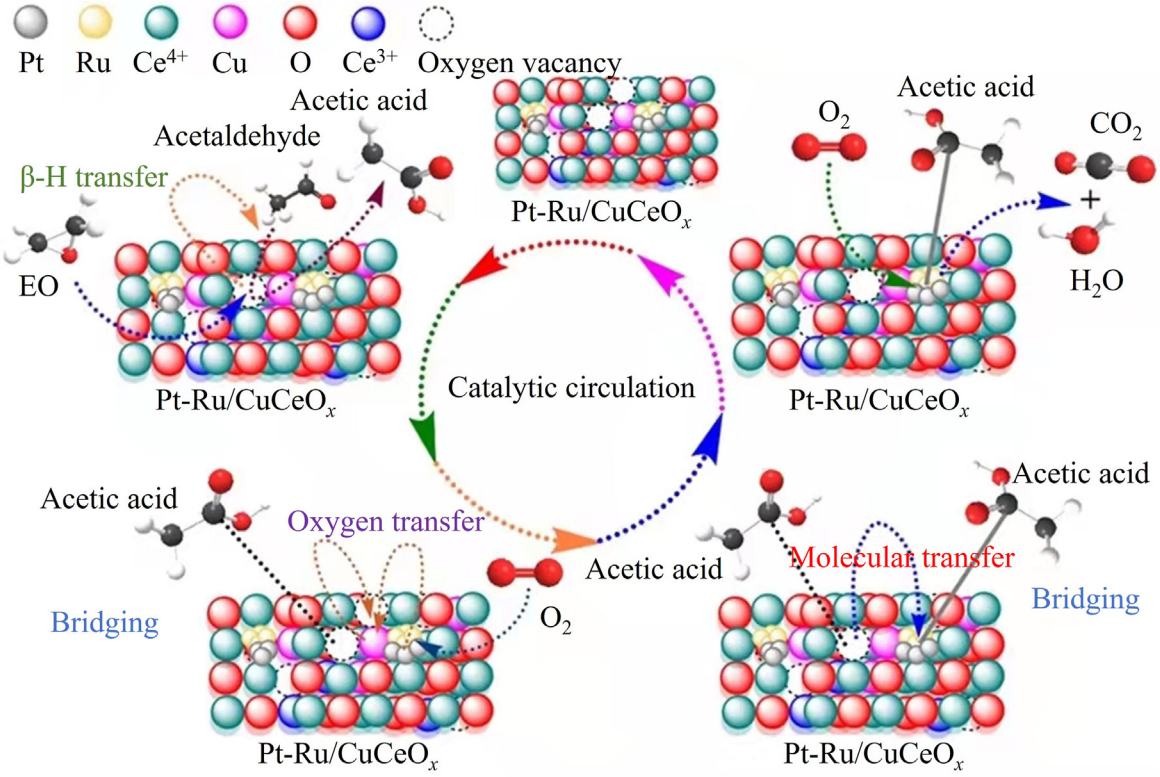

Fig. 7. Mechanism of EO catalytic oxidation over Pt-Ru/$CuCeO_x$ catalyst surface. The different intermediates are derived from the *in-situ* DRIFTs spectra of EO oxidation on the catalysts together with the GC-mass tests of the outlet gases in Fig. S4.

interface between the supported metal and the support by electron transfer and supplements the lattice oxygen consumed in the above reactions. Due to the presence of oxygen onions, the noble metal Pt-Ru nanoparticles have certain electronegativity, which induces acetic acid molecules to migrate to the active site of noble metal Pt-Ru nanoparticles. Finally, another molecular oxygen is co-adsorbed on the active sites of noble metal Pt-Ru nanoparticles and reacts with acetic acid to generate CO_2 and H_2O, and then the active sites on the surface of the catalyst are recovered. This process appears to follow the L-H catalytic mechanism. In short, the EO oxidation reaction on the surface of Pt-Ru/$CuCeO_x$ catalyst does not simply follow MvK or L-H catalytic mechanism, and both mechanisms may play significant roles in different stages of the reaction, based on the reaction conditions.

4. Conclusions

As mentioned above, the Pt-Ru bimetallic catalyst has a good catalytic activity and stability for EO oxidation, which can effectively degrade EO waste gas under temperature as low as 120 °C. XPS analyses show that the high activity may be related to the presence of RuO_x species, which enhances both the metal-support interaction and the low-temperature catalytic activity of Pt-Ru/$CuCeO_x$ catalyst for EO. In addition, when adsorbed on the surface of Pt-Ru/$CuCeO_x$ catalyst, EO oxidation does not follow a single catalytic mechanism, and the MvK catalytic mechanism and L-H catalytic mechanism may work at different stages during the catalytic oxidation of EO. At low temperature (T_{10}), EO is first converted to acetaldehyde and then to acetic acid, which follows the MvK catalytic mechanism. At higher temperature (T_{100}), the noble

metal Pt-Ru nanoparticles serve as the active sites, where the oxygen and acetic acid molecules are adsorbed and oxidized into CO_2 and H_2O, which follows the L-H catalytic mechanism. Accordingly, the adoption of bimetallic phase and modification of support prove to be a valid and universal way for improving VOCs abatement efficiency, and the applications to different VOCs can now be explored.

Declaration of competing interest

The authors declare that they have no conflict of interest.

Appendix A. Supplementary data

Supplementary data to this article can be found online at https://doi.org/10.1016/j.jre.2023.03.016.

References

1. Shao YQ. Current situation and marketing strategy of domestic ethylene oxide market. *Chem Enterp Manage*. 2021;(4):5 (in Chin.).
2. Sreejith LS, Sasi R. Residual ethylene oxide in medical devices: effects and estimation methods, an overview. *Trends Biomater Artif Organs*. 2020;34(1):7.
3. Sun B, Wen M, Ma X. Rapid absorption of ethylene oxide exhaust by catalytic hydration on acid zeolite catalysts. *Environ Technol Innov*. 2019;15, 100376.
4. Vkeng A, Lemanski MF, Kunin R. *Catalyst stabilizing additive in the hydrolysis of alkylene oxides*. US Patent: US 6156942 A; 2000.
5. Van Hal JW, Ledford JS, Zhang X. Investigation of three types of catalysts for the hydration of ethylene oxide (EO) to monoethylene glycol (MEG). *Catal Today*. 2007;123(1):310.
6. Wang F, Chen JL, Zhang B, Chen Q, He MY. Hydration reaction of ethylene oxide over modified silica gel. *Chin J Catal*. 2005;(5):355 (in Chin.).
7. Li YC, Yan SR, Qian LP, Yang WM. Effect of tin on Nb_2O_5/α-Al_2O_3 catalyst for ethylene oxide hydration. *J Catal*. 2006;241(1):173.
8. Li YC, Yan SR, Yang WM, Xie ZK. Effects of support modification on Nb_2O_5/α-Al_2O_3 catalyst for ethylene oxide hydration. *J Mol Catal Chem*. 2005;226(2):285.
9. Yang ZJ, Li YF, Wu QB, Ren N, Zhang YH, Liu ZP, et al. Layered niobic acid with self-exfoliatable nanosheets and adjustable acidity for catalytic hydration of ethylene oxide. *J Catal*. 2011;280(2):247.
10. Chen J, Jiang M, Xu W, Chen J, Jia H. Incorporating Mn cation as anchor to atomically disperse Pt on TiO_2 for low-temperature removal of formaldehyde. *Appl Catal, B*. 2019;259, 118013.
11. Jiang ZY, Jing MZ, Feng XB, Xiong JC, He C, Douthwaite M, et al. Stabilizing platinum atoms on CeO_2 oxygen vacancies by metal-support interaction induced interface distortion: mechanism and application. *Appl. Catal., B l.* 2020;278, 119304.
12. Santos VP, Carabineiro SAC, Tavares PB, Pereira MFR. Oxidation of CO, ethanol and toluene over TiO_2 supported noble metal catalysts. *Appl Catal, B*. 2010;99:198.
13. Liu YF, Zhou Y, Ke QL, Liu M, Zhou WX, Cui GH, et al. Enhanced catalytic oxidation of diluted ethylene oxide on Pt/CeO_2 catalyst under low temperature. *Appl. Catal., A*. 2020;639, 118642.
14. Kamiuchi N, Mitsui T, Muroyama H, Matsui T, Kikuchi R, Eguchi K. Catalytic combustion of ethyl acetate and nano-structural changes of ruthenium catalysts supported on tin oxide. *Appl Catal, B*. 2010;97(1):120.
15. Liu XW, Wang DS, Peng Q, Li YD. Bimetallic nanomaterials and catalysis. *Sci China Chem*. 2014;44(1):85 (in Chin.).
16. Fu XR, Liu Y, Yao WY, Wu ZB. One-step synthesis of bimetallic Pt-Pd/MCM-41 mesoporous materials with superior catalytic performance for toluene oxidation. *Catal Commun*. 2016;83:22.
17. Wang MM, Chen DY, Li NJ, Xu QF, Li H, He JH, et al. Highly efficient catalysts of bimetallic Pt−Ru nanocrystals supported on ordered ZrO_2 nanotube for toluene oxidation. *ACS Appl Mater Interfaces*. 2020;12(12), 13781−1.
18. Serna-Mata JH, Díaz-Guilléna JA, Rodríguez-Varelab FJ, Carrillo-Rodriguez JC, Alonso-Lemus LL, Garcia-Lobato MA. Nanostructured Pt-Ru catalyst supported on Si-containing ordered mesoporous carbon hollow spheres for the ethanol oxidation reaction. *ECS Trans*. 2022;108(7):59.
19. Mao XZ, Liu SR, Liu W, Wu XD, Liu S. A simple model catalyst study to distinguish the roles of different oxygen species in propane and soot combustion. *Appl Catal, B*. 2022;310, 121331.
20. Liu QL, Wu XQ, Han R, Pang CH, Xing S, Yang LZ, et al. Confined growth of Cu-doped CeO_2 nanostructures in boron-rich carbon frameworks for acetone oxidation. *ACS Appl Nano Mater*. 2021;4, 10275.
21. Shen YJ, Deng J, Han LP, Ren W, Zhang DS. Low-temperature combustion of toluene over Cu-doped $SmMn_2O_5$ mullite catalysts via creating highly active Cu^{2+}-O-Mn^{4+} sites. *Environ Sci Technol*. 2022;56, 104331.
22. Zhou Y, Gu QY, Qiu TZ, He X, Chen JQ, Qi RJ, et al. Ultrasensitive sensing of volatile organic compounds using a Cu-doped SnO_2-NiO p-n heterostructure that shows significant Raman enhancement. *Angew Chem Int Ed*. 2021;60(50), 26260.
23. Feng J, Zhang Y, Xiong W, Ding H, He B. Hydrogenolysis of glycerol to 1,2-propanediol and ethylene glycol over Ru-Co/ZrO_2 catalysts. *Catalysts*. 2016;6(4):51.
24. Mitsui T, Matsui T, Kikuchi R, Eguchi K. Low-temperature complete oxidation of ethyl Acetate over CeO_2-supported precious metal catalysts. *Top Catal*. 2009;52(5):464.
25. Weng SF, Xu YZ. *Fourier transform infrared spectroscopy. 3rd edn*. Beijing: Chemical Industry Press; 2017.
26. Zhang RD, Shi DJ, Liu N, Cao Y, Chen BH. Mesoporous SBA−15 promoted by 3d-transition and noble metals for catalytic combustion of acetonitrile. *Appl Catal, B*. 2014;146:79.
27. Chen CS, Lai YT, Chen TC, Chen CH, Lee JF, Hsu CW, et al. Synthesis and characterization of Pt nanoparticles with different morphologies in mesoporous silica SBA−15 for methanol oxidation reaction. *Nanoscale*. 2014;6(21), 12644.
28. Jiang ZY, Jing MZ, Feng XB, Xiong JC, He C, Douthwaite M, et al. Stabilizing platinum atoms on CeO_2 oxygen vacancies by metal-support interaction induced interface distortion: mechanism and application. *Appl Catal, B*. 2020;278(5), 119304.
29. Zou XL, Rui ZB, Song SQ, Ji HB. Enhanced methane combustion performance over $NiAl_2O_4$-interface-promoted Pd/γ-Al_2O_3. *J Catal*. 2016;338:192.
30. Zeng JL, Liu XL, Wang J, Lv HL, Zhu TY. Catalytic oxidation of benzene over MnO_x/TiO_2 catalysts and the mechanism study. *J Mol Catal Chem*. 2015;408:221.
31. He C, Jiang ZY, Ma MD, Zhang XD, Douthwaite M, Shi JW, et al. Understanding the promotional effect of Mn_2O_3 on micro-mesoporous hybrid silica nanocubic-supported Pt catalysts for the low-temperature destruction of methyl ethyl ketone: an experimental and theoretical study. *ACS Catal*. 2018;8(5):4213.
32. Tian MJ, Guo X, Dong R, Guo Z, Shi JW, Yu YK, et al. Insight into the boosted catalytic performance and chlorine resistance of nanosphere-like meso-macroporous $CrO_x/MnCo_3O_x$ for 1,2-dichloroethane destruction. *Appl Catal, B*. 2019;259, 118018.